GATING KINETICS OF BATRACHOTOXIN-MODIFIED SODIUM CHANNELS IN NEUROBLASTOMA CELLS DETERMINED FROM SINGLE-CHANNEL MEASUREMENTS

LI-YEN MAE HUANG
Marine Biomedical Institute, University of Texas Medical Branch, Galveston Texas 77550

NAVA MORAN AND GERALD EHRENSTEIN
Laboratory of Biophysics, National Institute of Neurological and Communicative Disorders and Stroke, National Institutes of Health, Bethesda, Maryland 20205

ABSTRACT We have observed the opening and closing of single batrachotoxin (BTX)-modified sodium channels in neuroblastoma cells using the patch-clamp method. The conductance of a single BTX-modified channel is ~10 pS. At a given membrane potential, the channels are open longer than are normal sodium channels. As is the case for normal sodium channels, the open dwell times become longer as the membrane is depolarized. For membrane potentials more negative than about −70 mV, histograms of both open-state dwell times and closed-state dwell times could be fit by single exponentials. For more depolarized potentials, although the open-state histograms could still be fit by single exponentials, the closed-state histograms required two exponentials. This data together with macroscopic voltage clamp data on the same system could be accounted for by a three-state closed-closed-open model with transition rates between these states that are exponential functions of membrane potential. One of the implications of this model, in agreement with experiment, is that there are always some closed BTX-modified sodium channels, regardless of membrane potential.

INTRODUCTION

Batrachotoxin (BTX), which is produced by the Colombian frog *Phyllobates aurotaenia*, is one of the most potent and specific activators of sodium channels. BTX-modified sodium channels activate at much more hyperpolarized potentials than do normal sodium channels (Albuquerque et al., 1971; Narahashi et al., 1971; Albuquerque et al., 1973; Khodorov, 1978) and do not exhibit either fast or slow inactivation (Khodorov, 1978; Huang et al., 1982). Thus BTX-modified sodium channels open persistently at the resting membrane potential. Therefore, in the presence of BTX, the isotope flux method can be used to probe the properties of sodium channels and to study the interactions between various pharmacological agents. Flux experiments carried out in cultured neuroblastoma cells indicate that BTX binds to the same receptor site as several other alkaloid toxins, such as veratridine and aconitine (Catterall, 1975; Catterall, 1977), but that the BTX receptor site is distinct from receptor sites for tetrodotoxin (Catterall, 1975), scorpion toxin (Catterall, 1977), and some local anesthetics (Huang and Ehrenstein, 1981).

A detailed voltage-clamp analysis of the action of BTX on these cultured neuroblastoma cells (Huang et al., 1982) indicated that BTX modifies sodium channels by (*a*) shifting the conductance-voltage curve ~50 mV in the hyperpolarizing direction with no change in its shape; (*b*) shifting the τ_m-voltage curve ~50 mV in the hyperpolarizing direction with a sixfold increase in the maximum value of τ_m; (*c*) changing the activation kinetics to first order; (*d*) eliminating fast inactivation; (*e*) eliminating slow inactivation.

One of the interesting properties of BTX-modified sodium channels is that its activation follows simple first-order kinetics, in contrast to the sigmoidal time course of normal sodium channels. Experiments on the gating properties of sodium channels (Armstrong and Bezanilla, 1977), on the single-channel behavior of sodium channels (Sigworth and Neher, 1980), and on the kinetics of sodium current after removal of inactivation (Oxford, 1981; Patlak and Horn, 1982) suggest that, upon depolarization, resting sodium channels must pass through several closed states in order to reach the open state. The first-order kinetics observed in the BTX-modified sodium channel under voltage clamp is consistent with a two-state (a closed state and an open state) kinetic model. An alternative possibility is that the BTX-modified sodium channel has additional states, that the overall reaction rate is a sum of exponentials with different weightings, and that the pattern of transition rates is such that one of the exponential components tends to dominate, as we previously suggested (Huang et al., 1982). If there are additional states, they are

more likely to be found by studying the opening and closing of single channels, because this allows the separation of the opening and closing processes.

We have studied the properties of BTX-modified sodium channels using single-channel techniques to obtain a better kinetic model and to determine how the fundamental transition rates vary with membrane potential. The model we seek must account for both the single-channel data and the macroscopic voltage-clamp data obtained with the same preparation (Huang et al., 1982). An additional goal is to gain some insight into the mechanism for the action of BTX and other channel-opening drugs.

An important advantage of studying the BTX-modified sodium channel is that it does not inactivate. Because the normal sodium channel inactivates with time, single-channel activity can only be elicited and measured during a short voltage pulse. Furthermore, the activation of normal sodium channels is coupled with inactivation (Goldman and Schauf, 1972; Armstrong and Bezanilla, 1977), and the time course of these two processes overlap (Aldrich et al., 1982; French and Horn, 1983). Thus it is very difficult to accurately determine activation parameters when inactivation is present. Because the BTX-modified sodium channel does not inactivate, it is possible to measure single-channel behavior at each membrane potential under relatively simple conditions for relatively long continuous periods.

Quandt and Narahashi (1982) have studied single-channel properties of sodium channels in the presence of BTX. They found that BTX prolongs the open state of the channel and decreases its single-channel conductance. In this paper, we report the voltage-dependence of opening and closing rates for a saturating concentration of BTX. This avoids the ambiguities and inaccuracies that may arise in resolving single-channel records of mixtures of normal and BTX-modified sodium channels. Only patches containing one channel were analyzed. Preliminary results of these studies have appeared in an abstract (Huang et al., 1983).

METHODS

Materials

The media and chemicals used were obtained from the following sources: Dulbecco-Vogt modification of Eagle's Minimal essential medium (DMEM) and newborn calf serum were from Grand Island Biological Company (Grand Island, NY). BTX was kindly supplied by Dr. John Daly (Laboratory of Digestive Diseases, National Institute of Arthritis, Diabetes, Digestive and Kidney Diseases). Prostaglandin El, theophylline, hypoxanthine, aminopterin, and thymidine are from Sigma Chemical Corporation (St. Louis, MO). Tetraethylammonium chloride is from Eastman Kodak Company (Rochester, NY).

Cell Culture

NG108-15 cells, which are neuroblastoma glioma hybrid cells derived by fusion of mouse neuroblastoma clone N18TG2 with rat glioma clone C6BU-1 were used in the experiments. Stock culture of NG108-15 was grown in DMEM containing 5% newborn calf serum, 100 μM hypoxanthine, 1 μM aminopterin, and 16 μM thymidine at 36.5°C in a humidified atmosphere of 10% CO_2/90% air. To induce neuronal differentiation, cells used for experiments were cultured in the above medium, to which 1 μM prostaglandin El and 1 mM theophylline were added for 5–7 d before use. Cells treated in this way have more negative membrane potential (< -70 mV) and are more excitable than the untreated cells.

Electrophysiology

Experiments were performed at room temperature (20°–23°C). The external solution contained 130 mM NaCl, 0.8 mM $MgCl_2$, 5.4 mM KCl, and 20 mM HEPES. 30 mM tetraethylammonium and 0.5 mM Ca^{2+} were added in the bath medium to reduce the K^+-, Ca^{2+}-, and Ca^{2+}-dependent K currents. The pH of the external solution was adjusted to 7.4 with 14 mM Tris base.

BTX was stored in ethanol at 2 mM concentration and was added to the bath media immediately before use. The high concentration of BTX stock solution was used to reduce the final concentration of ethanol present in the bath solution. A high concentration of ethanol changes the opening and closing rates of sodium channels (unpublished observations). A saturating concentration of BTX (2–5 μM) was added to the bath for at least 45 min before starting the experiments. This length of time is required to allow the BTX binding to reach equilibrium. Because BTX activates sodium channels at resting potential, the internal sodium ion concentration increases during this preincubation period until it is equal to the sodium ion concentration in the bath. Independent measurements of membrane potential using microelectrodes indicated that the resting potential is ~0 mV.

An extracellular patch-clamp system from List Electronics (West Germany) was used to record the single-channel current. The patch electrode was fabricated according to the method of Hamill et al. (1981) and was coated with wax. The tip diameter of the electrode was <1 μm and its resistance was 3–5 MΩ . The solution in the patch pipet was the same as the external solution. The potential was measured using Ag/AgCl electrodes from W. P. Instruments, Inc. (New Haven, CT).

The culture dish was mounted on the stage of a phase-contrast microscope. The single-channel current was recorded by establishing a gigaohm seal (10–50 GΩ) between the electrode and the cell membrane. Cell-attached and inside-out recordings were then made. Unless otherwise noted, all the results in this paper were obtained from cell-attached recordings.

Membrane potentials were held at the levels indicated in the Results Section for a few minutes before recording. The currents were filtered through a four-pole low-pass Krohn-Hite filter at a corner frequency of 1 kHz, and were then digitalized and recorded continuously on DEC11/20 digital tape. The data were sampled at 128 μs intervals. The results were analyzed by displaying the current records on a Matrox video terminal and visually determining channel amplitudes, open dwell times, and closed dwell times.

RESULTS

Single-channel Conductance of BTX-modified Sodium Channels

Because BTX eliminates inactivation of sodium channels, we were able to record relatively long trains of channel events under steady-state conditions. Fig. 1 shows the opening and closing of a single BTX-modified sodium channel at several different membrane potentials. The fraction of time the channel is open increases with membrane depolarization. Within the time resolution of our system, the open BTX-modified sodium channel does not flicker.

A histogram of the current amplitude corresponding to

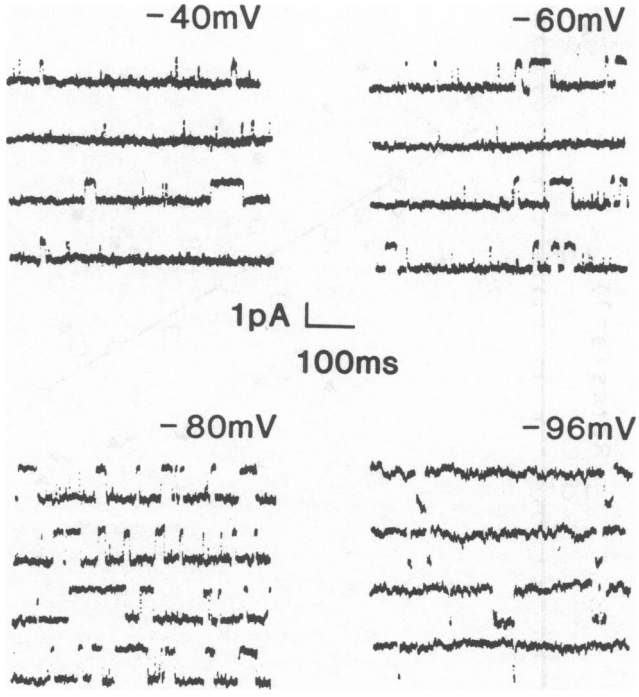

FIGURE 1 Single-channel current jumps recorded from cell-attached patch at indicated membrane potentials. Downward deflections indicate channel opening (and inward current).

individual opening and closing events at one particular membrane potential is shown in Fig. 2. The experimental data are reasonably fit by a Gaussian distribution curve. Similar curves were obtained for each experimental membrane potential, and the mean current corresponding to each potential was determined. The mean currents are plotted as a function of membrane potential in Fig. 3, which shows that the single-channel current-voltage curve is approximately linear within the potential range studied.

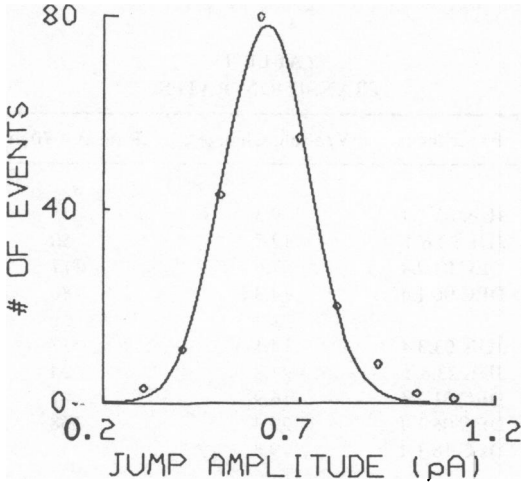

FIGURE 2 Histogram of current-jump amplitudes at −40 mV. Symbols: experimental data. Curve: Gaussian distribution [$g = A \exp(-((x - u)/s)^2)$] fit with the parameters: $u = 0.62$ pA, $s = 0.15$ pA. Note the single modality of this distribution.

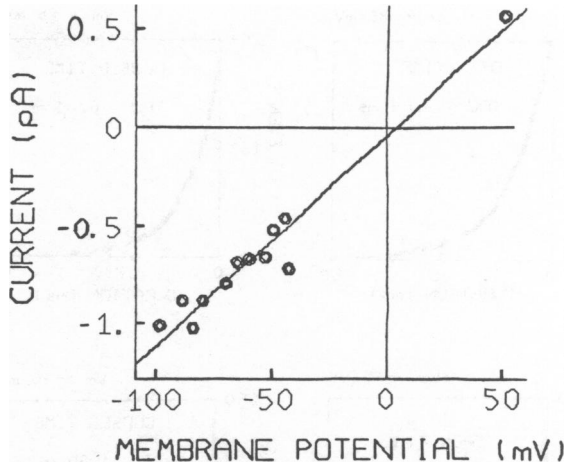

FIGURE 3 Current-voltage curve of single-channel current jumps. Symbols: experimental data. Curve: fit with unit conductance = 10.7 ± 0.7 pS and reversal potential = 4.1 ± 4.6 mV.

The conductance of the BTX-modified sodium channel obtained from the slope of this curve is ~10 pS.

Histograms for Opening and Closing Rates

In this paper we have analyzed only those records where a single channel was present in the patch, as evidenced by the absence of two simultaneously open channels. This avoids ambiguity in deciding which channel opened or closed—information needed to obtain dwell-time histograms.

For both open dwell times and closed dwell times, histograms of the cumulative number of events longer than time t are shown as a function of t in Fig. 4. The cumulative histograms are integrals of the dwell-time histograms, and should be exponential if the dwell times are exponentially distributed. The reason for plotting the cumulative histograms rather than the dwell-time histograms is simply to utilize the additional smoothing inherent in integration.

Fig. 4 shows dwell times in the open state and in the closed state for two different membrane potentials. In three of these four cases, the data can be fit by a single exponential; in the other case, the sum of two exponentials is required to fit the data. In our experiments, single-exponential fits were found for open-state dwell times (corresponding to closing rates) at all membrane potentials. For closed-state dwell times (corresponding to opening rates), single-exponential fits were found for relatively negative membrane potentials (< -70 mV), but the sum of two exponentials is required to fit the data for relatively positive membrane potentials.

For each experiment, cumulative histograms for open dwell-times and for closed dwell-times were plotted and were fit to one exponential or to the sum of two exponentials, as required. All of the experimental closing rates are shown on a logarithmic scale as a function of membrane potential in Fig. 5. For each experiment, the points can be reasonably well fit by a straight line,

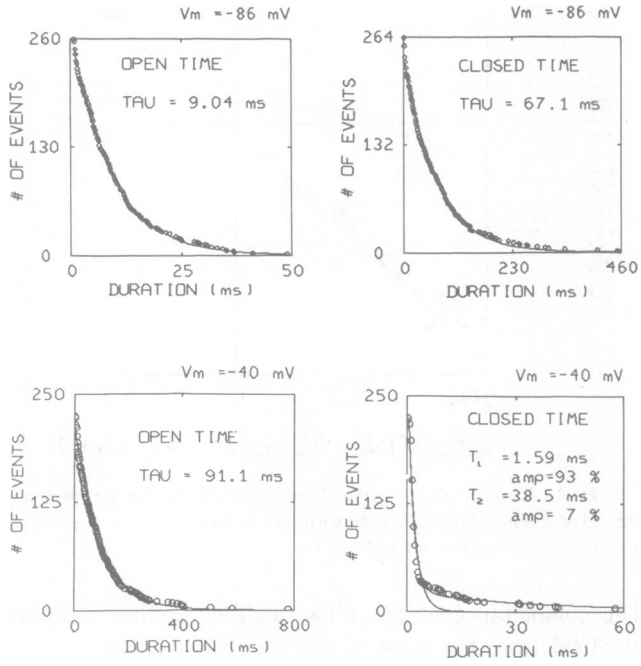

FIGURE 4 Cumulative dwell-time histograms for open channels and closed channels at two membrane potentials. Symbols: experimental data. Curves: for each histogram, best-fit single exponential is shown; for closed-time histogram at $V_m = -40$ mV, the best-fit sum of two exponentials is also shown. Note the deviation from single exponential in the latter case.

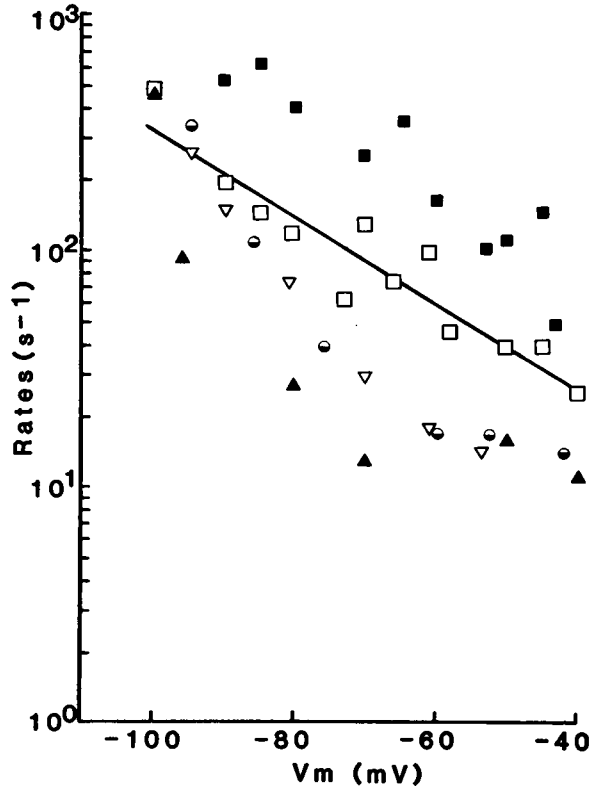

FIGURE 5 Voltage dependence of microscopic closing rates. Symbols: (open time constant)$^{-1}$ obtained by fitting single exponential to dwell-time histograms. Different symbols stand for separate experiments. Solid line (—): best fit to the data from Experiment JUL 23.6*A*, represented here by open squares (□).

indicating that the closing rate is an exponential function of membrane potential. The best-fit straight lines were determined by least squares for each experiment. The lines are approximately parallel, but there is a relatively large displacement between them. As shown in Table I, the slopes of these lines vary by about a factor of two, but the amplitudes at −70 mV vary about tenfold.

The dependence of opening rates on membrane potential is shown in Fig. 6 *a* for all the experiments. For hyperpolarized potentials, the closed-time histograms can be described by single exponentials, and hence there is a single opening rate for each voltage. These opening rates increase exponentially with membrane potential. For membrane potentials more positive than about −70 mV, two-exponential closed-time histograms were observed; thus, a pair of opening rates is associated with each voltage in this region. The faster opening rates have approximately the same exponential voltage dependence as the opening rates in the hyperpolarized region, whereas the slower opening rates decrease exponentially with membrane potential. In Fig. 6 *a*, filled circles correspond to single opening rates and half-filled circles correspond to pairs of opening rates. The overall pattern of the data of Fig. 6 *a* is shown schematically in Fig. 6 *b*. Fig. 6 *c* shows opening rates for one experiment. The ratio of the amplitude of the slower exponential component of the cumulative opening rate histogram to the amplitude of the faster exponential component is shown in Fig. 7.

Determination of Transition Rates for Three-state Model

The fact that some of the histograms could not be fit by a single exponential indicates that more than two states are required to explain the gating mechanism of this system

TABLE I
TRANSITION RATES

Rate	Experiment	mV/*e*-fold Change	Rate at −70 mV
			s^{-1}
α	JUN 03.3*A*	9.3	45
	JUL 23.6*A*	12.7	50
	DEC 01.2*A*	7.6	117
	DEC 06.1*A*	14.3	80
β	JUN 03.3*A*	−14.1	37
	JUL 23.6*A*	−23.8	94
	DEC 01.2*A*	−16.9	47
	DEC 06.1*A*	−20.4	268
	DEC 18.1*A*	−19.6	33
γ	JUL 23.6*A*	−21.3	91
	DEC 18.1*A*	−30.3	71
δ	JUL 23.6*A*	9.5	4

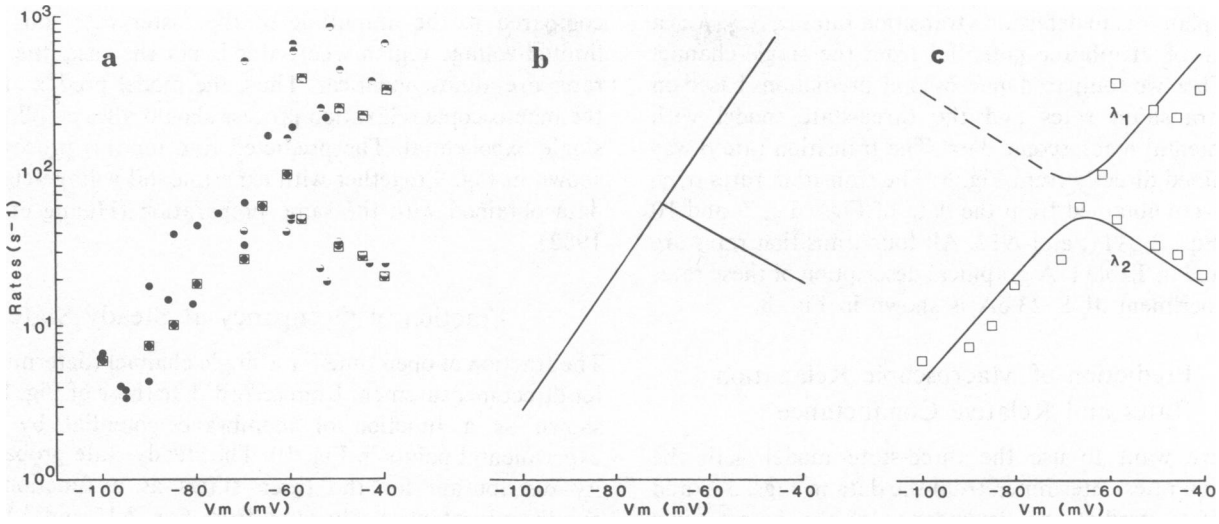

FIGURE 6 Voltage dependence of microscopic opening rates. *a*, (closed time constant)$^{-1}$ obtained by fitting closed-time histograms with either single exponentials (filled circles, •) or sum of two exponentials (half-filled circles). Same experiments as in Fig. 5. Open squares (□) surround the circles for the experiment described by open squares in Fig. 5. *b*, schematic representation of data. *c*, symbols: opening rates for experiment described by open squares in Fig. 5 and in Fig. 6 *a*. Curves: opening rates λ_1 and λ_2, calculated from transition rates α, γ, and δ, and Eq. (2). Dashed curve represents rates associated with an exponential term with a relatively insignificant amplitude (<1% of other exponential amplitude at same voltage).

over the range of membrane potentials examined. Therefore, we tried to fit our experimental data to the following three-state model

$$C \underset{\delta}{\overset{\gamma}{\rightleftharpoons}} C \underset{\beta}{\overset{\alpha}{\rightleftharpoons}} O$$

where C is a closed state and O is an open state.

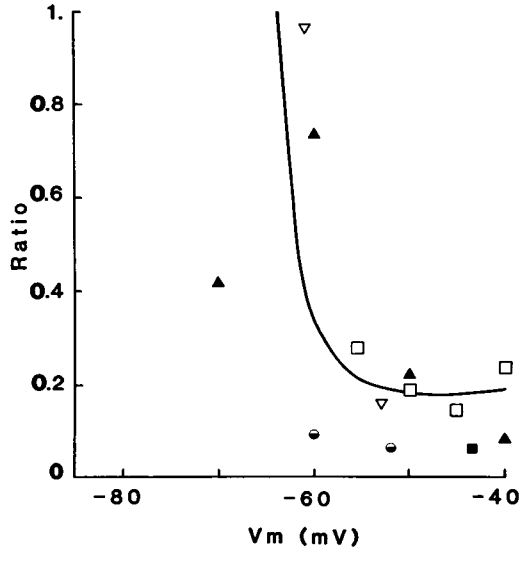

FIGURE 7 Ratio of the amplitude of the slow exponential to the amplitude of the fast exponential describing the microscopic opening rates. Symbols: experimental values obtained by fitting closed-time cumulative histograms with sum of two exponentials in voltage range where single exponential was inadequate. Same experiments as in Fig. 5 and 6 *b*. Curve: ratio calculated from Eq. 3., using the transition rates α, γ, and δ from Experiment JUL 23.6*A*.

There are four rates associated with transitions between the discrete states in the above model. To distinguish between these rates and the overall rates that would be observed experimentally, we call the rates α, β, γ, δ transition rates, we use the lower case Greek letters λ_1 and λ_2 to describe the microscopic opening rates, and we use the upper case Greek letters Λ_1 and Λ_2 to describe the macroscopic relaxation rates.

The microscopic opening and closing rates and the macroscopic relaxation rates are all functions of the transition rates. For the three-state model above, there are in general two macroscopic rates, implying two exponentials for the time course to reach steady state under voltage clamp. These macroscopic rates depend on the transition rates as follows (cf. Appendix)

$$\Lambda_1,\Lambda_2 = \tfrac{1}{2}[\alpha + \beta + \gamma + \delta \pm \sqrt{(\alpha + \beta + \gamma + \delta)^2 - 4(\alpha\gamma + \beta\delta + \beta\gamma)}]. \quad (1)$$

For the same kinetic model, the single-channel microscopic closing rate is simply equal to the transition rate, β. There are two microscopic opening rates, and these are related to the transition rates as follows (Colquhoun and Hawkes, 1981)

$$\lambda_1,\lambda_2 = \tfrac{1}{2}[\alpha + \gamma + \delta \pm \sqrt{(\alpha + \gamma + \delta)^2 - 4\alpha\gamma}]. \quad (2)$$

This relation is the same as the relation for the macroscopic rates for the special case that $\beta = 0$. The reason for this is that the microscopic opening rates, as determined from the closed-time histograms, correspond to a process that does not consider the fate of a channel after it opens.

Our plan was to determine transition rates α, β, γ, δ as a function of membrane potential from the single-channel data. Then we compared macroscopic predictions based on these transition rates and the three-state model with experimental macroscopic data. The transition rate β was determined directly from Fig. 5. The transition rates α, γ, and δ were obtained from the data of Figs. 6 *c*, 7, and 10 using Eqs. 2, A11, and A12. All four transition rates are tabulated in Table I. A graphical description of these rates for Experiment JUL 23.6A is shown in Fig. 8.

Prediction of Macroscopic Relaxation Rates and Relative Conductance

Next we want to use the three-state model with the transition rates determined from the data in Figs. 5–7 and Fig. 10 to predict the dependence of the macroscopic relaxation rates on membrane potential. Because the three-state model in general gives the sum of two exponentials for the macroscopic relaxation rate, it is necessary to consider the expression for the ratio of the amplitudes of the macroscopic rates (cf. Eq. A19) as well as the expression (Eq. 1) for the rates themselves.

When the values of the transition rates determined from microscopic data (cf. Fig. 8) are substituted into the above expression for the amplitude ratio of the two macroscopic relaxation rates, it turns out that for almost the entire voltage range the amplitude of the slower rate is negligible compared to the amplitude of the faster rate. For the limited-voltage region where this is not the case, the two rates are almost identical. Thus, the model predicts that the macroscopic relaxation process should always follow a single exponential. The predicted rate for this process is shown in Fig. 9 together with experimental voltage-clamp data obtained with the same preparation (Huang et al., 1982).

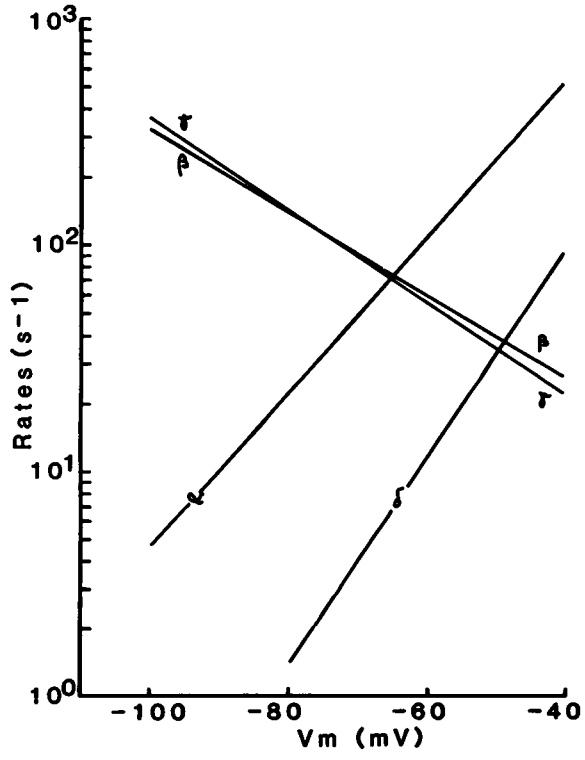

FIGURE 8 Voltage dependence of microscopic transition rates for C–C–O model.

Fraction of Occupancy at Steady State

The fraction of open time for a single channel (determined for direct measurement from records like those of Fig. 1) is shown as a function of membrane potential by the experimental points in Fig. 10. The steady-state probability distribution for the three states as a function of membrane potential calculated from Eqs. A12 and A13 is shown by the curves in Fig. 10. There is good agreement between the experimental points and the curve calculated from the C-C-O model.

DISCUSSION

There are two primary purposes of this study. One purpose is to obtain a better understanding of the mechanism by which BTX modifies sodium channels. The other purpose is to determine a kinetic model for a voltage-gated channel that is consistent with both single-channel data and macroscopic voltage clamp data on the same preparation over a considerable voltage range. The BTX-modified sodium channel in neuroblastoma cells is particularly convenient for both purposes because ionic flux studies and voltage clamp studies have already been performed on this preparation and because it does not inactivate.

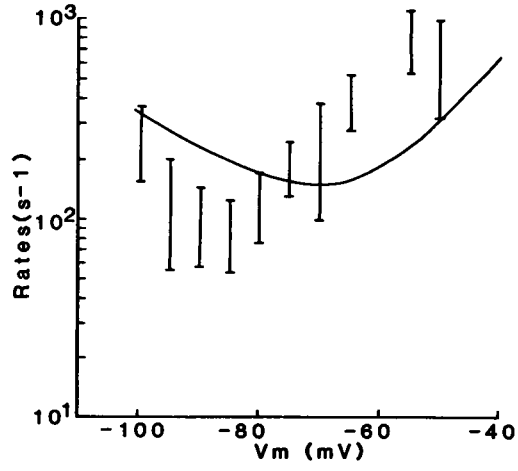

FIGURE 9 Voltage dependence of macroscopic relaxation rates. Bars: range of values of (time constant)$^{-1}$ obtained from macroscopic voltage-clamp experiments (Huang et al., 1982), by fitting a single exponential to the rising phase of sodium conductance elicited by a depolarizing pulse. Curve: calculated from Eq. 1 and transition rates determined for Experiment JUL 23.6*A*.

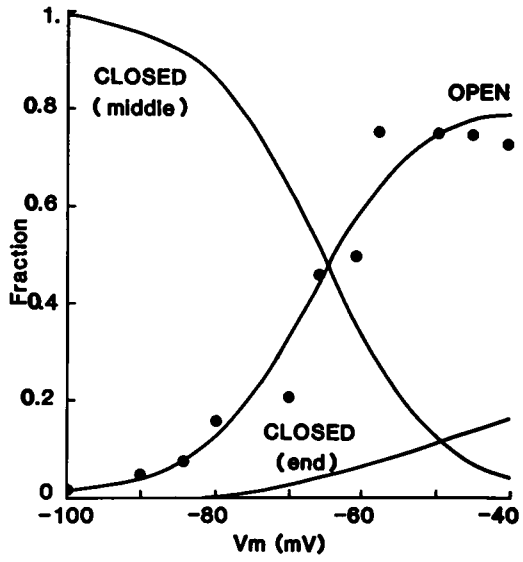

FIGURE 10 Voltage dependence of fraction of occupancy at steady state. Symbols: experimental values of fraction of open time determined for Experiment JUL 23.6A. Curves: fractions for each of the three states in the C–C–O model calculated from Eqs. A12 and A13 using the transition rates determined from the same experiment.

Usefulness of the Single-Channel Studies

The single-channel conductance that we measured for BTX-modified sodium channels in neuroblastoma cells is ~10 pS. By comparison, Khodorov et al. (1981) reported a value of 2–3 pS in frog node based on noise measurements and Quandt and Narahashi (1982) reported a value of 2 pS in neuroblastoma cells based on single-channel measurements. This apparent discrepancy may be due to the higher concentration of calcium used in those studies which found lower conductance, especially in view of the effect of increased calcium on rectification of the single-channel current-voltage curve recently reported by Yamamoto et al. (1983). Khodorov et al. (1981) and Quandt and Narahashi (1982) used 1.5–1.8 mM calcium, whereas we used 0.5 mM calcium.

In addition to providing a measurement of the conductance of a single channel, the single-channel method has several other advantages. One of these is that it provides an opportunity for determining the variability of the channel parameters. As shown in Fig. 5 and Table I, the most variability was found in the amplitude of the transition rate, β. We do not know whether this variability is related to variations between cells or whether there are large variations in channel properties even within the same cell. This is an interesting area for future investigation.

The present study of the single-channel kinetics of the BTX-modified sodium channel shows that, in the depolarized region, there is a second exponential opening rate with relatively small amplitude. It is interesting to note that the ability to detect this second exponential depends both on the single-channel method and on the large number of events that can be analyzed with a system whose recording time is several orders of magnitude longer than the channel opening or closing time. By contrast, the rates of EIM channels are about three orders of magnitude slower than the rates of sodium channels, and relatively few EIM channel events were analyzed for each experiment (Ehrenstein et al., 1974). Thus, departures from a two-state model comparable in magnitude to those reported here might not have been detected.

The observation of the second exponential in the closed-time histograms led to a three-state model. As shown in Fig. 9, the three-state model, together with parameters determined from single-channel data, provide a reasonable qualitative fit to the macroscopic relaxation times. The main discrepancy is that the minimum of the predicted curve is shifted ~15 mV toward positive potentials. Part of this discrepancy may be caused by the difficulty in making absolute voltage measurements with a cell-attached patch clamp. From our microelectrode measurements of resting potentials in cells without patch electrodes, we estimate the uncertainty of absolute potential to be <10 mV. Another part of the discrepancy may be caused by the variability of the transition rates from channel to channel. In any event, both the amplitude of the theoretical curve and its general shape are consistent with the experimental macroscopic data.

As shown in Fig. 10, the voltage dependence of the fraction of channels in the open state has the same general shape as the macroscopic conductance-voltage curve (Huang et al., 1982). As in Fig. 9, the main discrepancy in Fig. 10 is that the curve based on single-channel data is shifted toward positive potentials.

Although there is reasonably good agreement between the single-channel and macroscopic data, it is important to note that only the single-channel (microscopic) data provided information about the existence of the third state and its properties. The macroscopic data alone could be fit by a two-state model as well as by the three-state model.

Exponential Voltage Dependence of Transition Rates

The single-channel data shown in Figs. 5 and 6 were fit with the C–C–O model and the transition rates shown in Fig. 8. These transition rates were all chosen to be exponential functions of membrane potential because of the form of some of the experimental data. The good fits in Figs. 5, 6, 7, 9, and 10 provide stronger support for these choices.

An exponential voltage dependence is what would be expected if the energy difference between discrete states of the channel corresponded simply to the energy of charge movement. An exponential voltage dependence of transition rates between states may, in fact, be a general feature of electrically excitable channels. For example, it corresponds to the results of previous work on a voltage-gated channel (EIM) in bilayers for the simpler case of a two-state model (Ehrenstein et al., 1970; Ehrenstein et al., 1974).

The simplest type of model that might account for the second exponential opening rate for the BTX-modified channel is a three-state model with two closed states and one open state. There are, in fact, two models of this type: the C–C–O model that we have used and a C–O–C model, where the open state lies between two closed states. Although we cannot rule out the C–O–C model, we prefer the C–C–O model. The reason for our preference is that the C–C–O model leads to transition rates that are simple exponential functions of membrane potential and have a simple physical interpretation, as discussed above. By contrast, the transition rates calculated from the C–O–C model are complex functions of membrane potential.

Significance of C–C–O Model

From the slopes of the curves in Fig. 8, we can estimate the charge movement between the states of the C–C–O model. From the middle closed state to the open state, about four charges cross the membrane, in rough agreement with our estimate of five charges from the macroscopic data (Huang et al., 1982). From the middle closed state to the other closed state, the number of charges crossing the membrane is also about four. In addition, the direction of movement of the charges in leaving the middle closed state is the same regardless of whether the transition is to an open state or to a closed state. This implies that at hyperpolarized membrane potentials, the middle state in the C–C–O model is preferentially populated relative to the other closed state. By contrast, evidence from kinetic measurements and from gating charge measurements indicates that for normal sodium channels the closed states furthest from the open state are preferentially populated at hyperpolarized membrane potentials (Armstrong and Bezanilla, 1977; Armstrong and Gilly, 1979).

Fig. 10 shows another implication of the C–C–O model. The fraction of channels that is open increases with increasing voltage, but saturates at ~80%. Also, the BTX-modified channel amplitude is about 70% of the unmodified channel amplitude (unpublished observations). Therefore, BTX would be expected to reduce the macroscopic sodium current by ~50%. Indeed, voltage clamp studies show that BTX causes ~50% reduction in maximum sodium current (Huang et al., 1982). For other alkaloid neurotoxins, such as aconitine and veratridine, the maximum sodium current is even more reduced (Campbell, 1982). A possible explanation for this further reduction in current is that the binding of these drugs results in an increased population of the end closed state and a decreased population of the open state. The fraction of channels in the open state would then saturate at lower values.

APPENDIX

C–C–O Kinetic Model

$$C \underset{\delta}{\overset{\gamma}{\rightleftharpoons}} C \underset{\beta}{\overset{\alpha}{\rightleftharpoons}} O$$

To relate experimentally measured kinetic parameters to the transition rates in the above model, it is convenient to make the following definitions:

$F_i(t)$ = fraction of channels in ith state.
$F_{i\infty}$ = fraction of channels in ith state at $t = \infty$.
$f_i(t) = F_i - F_{i\infty}$.
State 1 = open state.
State 2 = right-hand closed state.
State 3 = left-hand closed state.

By writing the rate equations for this system in terms of f_i, we can obtain a homogeneous set of equations, since $f_1 + f_2 + f_3 = 0$.

$$\dot{f}_1 = -\beta f_1 + \alpha f_2 \tag{A1}$$

$$\dot{f}_2 = (\beta - \gamma) f_1 - (\alpha + \gamma + \delta) f_2 \tag{A2}$$

These equations are most conveniently solved by assuming a trial solution of the form $f_i = a_{ij} e^{-\lambda_j t}$ and writing the resultant equations in matrix form $(M + \lambda I) f = 0$ where

$$M = \begin{pmatrix} -\beta & +\alpha \\ \beta - \gamma & -\alpha - \gamma - \delta \end{pmatrix}.$$

The eigenvalues, Λ, for these equations can be found by solving the characteristic equation (Bellman, 1953).

For the macroscopic case,

$$\Lambda_{1,2} = \tfrac{1}{2}[\alpha + \beta + \gamma + \delta \pm \sqrt{(\alpha + \beta + \gamma + \delta)^2 - 4(\alpha\gamma + \beta\delta + \beta\gamma)}]. \tag{A3}$$

For the microscopic case, the opening-rate histograms are obtained by measuring the time duration between a closing event and an opening event. Thus, the opening rate histograms are based on the C–C–O model with $\beta = 0$, and the microscopic opening rates can be found by letting $\beta = 0$ in the above equation:

$$\lambda_{1,2} = \tfrac{1}{2}[\alpha + \gamma + \delta \pm \sqrt{(\alpha + \gamma + \delta)^2 - 4\alpha\gamma}]. \tag{A4}$$

The coefficients a_{ij} can also be found by standard methods (Bellman, 1953) if the initial conditions are known.

For the microscopic case, at $t = 0$, $F_1 = 0$ and $F_2 = 1$. Also, since the opening-rate histograms are based on waiting until all channels open, $F_{1\infty} = 1$ and $F_{2,\infty} = 0$. Thus, the initial conditions are

$$f_1(0) = F_1(0) - F_{1\infty} = 0 - 1 = -1 \tag{A5}$$

$$f_2(0) = F_2(0) - F_{2\infty} = 1 - 0 = +1. \tag{A6}$$

For these initial conditions,

$$a_{21} = \frac{\lambda_1(\alpha - \lambda_2)}{\alpha(\lambda_1 - \lambda_2)} \tag{A7}$$

$$a_{22} = \frac{\lambda_2(\lambda_1 - \alpha)}{\alpha(\lambda_1 - \lambda_2)}. \tag{A8}$$

For the opening-rate histogram, the opening rate is proportional to F_2 (which is equal to f_2). For the cumulative opening-rate histogram, we must consider the time integral of $f_2(t)$ from t to ∞.

$$\int_t^\infty f_2(t)dt = \frac{\alpha - \lambda_2}{\lambda_1 - \lambda_2} e^{-\lambda_1 t} + \frac{\lambda_1 - \alpha}{\lambda_1 - \lambda_2} e^{-\lambda_2 t}. \tag{A9}$$

Define R_{mic} as the ratio of the amplitude of the slower exponential component of the cumulative opening-rate histogram to the amplitude of the faster exponential component. Then,

$$R_{mic} = \frac{\alpha - \lambda_1}{\lambda_2 - \alpha}. \tag{A10}$$

If the expressions for λ_1 and λ_2 in terms of the transition rates are substituted into the above equation, the result is

$$R_{mic} = \frac{\alpha - \gamma - \delta - \sqrt{(\alpha + \gamma + \delta)^2 - 4\alpha\gamma}}{\gamma + \delta - \alpha - \sqrt{(\alpha + \gamma + \delta)^2 - 4\alpha\gamma}}. \quad \text{(A11)}$$

For the macroscopic case, at the holding potential for voltage clamp experiments (−110 mV), β and γ are much larger than α and δ, as shown in Fig. 8. Thus, to a very good approximation, at $t = 0$, $F_1 = 0$ and $F_2 = 1$. At steady state,

$$F_{1\infty} = \frac{\alpha\gamma}{\alpha\gamma + \beta\gamma + \beta\delta} \quad \text{(A12)}$$

$$F_{2\infty} = \frac{\beta\gamma}{\alpha\gamma + \beta\gamma + \beta\delta}. \quad \text{(A13)}$$

Thus, the initial conditions are

$$f_1(0) = F_1(0) - F_{1\infty} = -\frac{\alpha\gamma}{\alpha\gamma + \beta\gamma + \beta\delta} \quad \text{(A14)}$$

$$f_2(0) = F_2(0) - F_{2\infty} = \frac{\alpha\gamma + \beta\delta}{\alpha\gamma + \beta\gamma + \beta\delta}. \quad \text{(A15)}$$

For these initial conditions,

$$a_{11} = \frac{\alpha}{(\Lambda_1 - \Lambda_2)}\left(\frac{\gamma\Lambda_2}{\alpha\gamma + \beta\gamma + \beta\delta} - 1\right) \quad \text{(A16)}$$

$$a_{12} = \frac{\alpha}{(\Lambda_1 - \Lambda_2)}\left(1 - \frac{\gamma\Lambda_1}{\alpha\gamma + \beta\gamma + \beta\delta}\right). \quad \text{(A17)}$$

In voltage clamp experiments, the conductance is proportional to F_1, and the time-dependent components of F_1 are equal to the time-dependent components of f_1.

Define R_{mac} as the ratio of the amplitude of the slower exponential component of the conductance change to the amplitude of the faster component. Then,

$$R_{mac} = \frac{a_{12}}{a_{11}} \quad \text{(A18)}$$

$$R_{mac} = \frac{\alpha\gamma + \beta\gamma + \beta\delta - \gamma\Lambda_1}{\gamma\Lambda_2 - \alpha\gamma - \beta\gamma - \beta\delta}. \quad \text{(A19)}$$

We wish to thank Ms. Janice Johnson for valuable technical assistance.

L. M. Huang wishes to acknowledge the support of part of her work by a New Investigator Award #7 R23 NS19352/01 from the National Institute of Neurological and Communicative Disorders and Stroke, National Institutes of Health.

Received for publication 4 May 1983 and in final form 14 June 1983.

REFERENCES

Albuquerque, E. X., J. W. Daly, and B. Witkop. 1971. Batrachotoxin: chemistry and pharmacology. *Science (Wash., DC)*. 172:995–1002.

Albuquerque, E. X., I. Seyama, and T. Narahashi. 1973. Characterization of batrachotoxin-induced depolarization of the squid giant axon. *J. Pharmacol. Exp. Ther.* 184:308–314.

Aldrich, R. W., D. P. Corey, and C. F. Stevens. 1982. Stochastic analysis of the kinetics of single sodium channels. Abstracts Society for Neuroscience. 8:727.

Armstrong, C. M., and F. Bezanilla. 1977. Inactivation of sodium channels. II. Gating current experiments. *J. Gen. Physiol.* 70:567–590.

Armstrong, C. M., and W. F. Gilly. 1979. Fast, and slow steps in the activation of sodium channels. *J. Gen. Physiol.* 74:691–711.

Bellman, R. 1953. Stability theory of differential equations.. McGraw-Hill, Inc. New York.

Campbell, D. T. 1982. Modified kinetics and selectivity of sodium channels in frog skeletal muscle fibers treated with aconitine. *J. Gen. Physiol.* 80:713–731.

Catterall, W. A. 1975. Activation of action potential sodium ionophores of cultured neuroblastoma cells by veratridine and batrachotoxin. *J. Biol. Chem.* 250:4053–4059.

Catterall, W. A. 1977. Activation of the action potential sodium ionophore by neurotoxins: an allosteric model. *J. Biol. Chem.* 252:8669–8676.

Colquhoun, D., and A. G. Hawkes. 1981. On the stochastic properties of single ion channels. *Proc. R. Soc. Lond. B Biol. Sci.*. 205–235.

Ehrenstein, G., R. Blumenthal, R. Lattore, and H. Lecar. 1974. Kinetics of opening and closing of individual excitability-inducing material channels in a lipid bilayer. *J. Gen. Physiol.* 63:707–721.

Ehrenstein, G., H. Lecar, and R. Nossal. 1970. The nature of the negative resistance in bimolecular lipid membranes containing excitability-inducing material. *J. Gen. Physiol.* 55:119–133.

French, R.J., and R. Horn. 1983. Sodium channel gating: models, mimics, and modifiers. *Annu. Rev. Biophys. Bioeng.* In press.

Goldman, L., and C. L. Schauf. 1972. Inactivation of the sodium current in *Myxicola* giant axons. Evidence for coupling to the activation process. *J. Gen. Physiol.* 59:659–675.

Hamill, O. P., A. Marty, E. Neher, B. Sakmann, and F. J. Sigworth. 1981. Improved patch-clamp techniques for high-resolution current recording from cells and cell-free membrane patches. *Pflügers Arch. Eur. J. Biol.* 391:85–100.

Huang, L. -Y. M., and G. Ehrenstein. 1981. Local anesthetics QX 572, and benzocaine act at separate sites on the batrachotoxin-activated sodium channel. *J. Gen. Physiol.* 77:137–153.

Huang, L. -Y. M., N. Moran, and G. Ehrenstein, G. (1982). Batrachotoxin modifies the gating kinetics of sodium channels in internally perfused neuroblastoma cells. *Proc. Natl. Acad. Sci. USA.* 79:2082–2085.

Huang, L. -Y. M., N. Moran, and G. Ehrenstein. 1983. Gating kinetics of batrachotoxin-modified sodium channels in neuroblastoma cells determined from single-channel measurement. *Biophys. J.* 41(2,Pt.2):50 *a*. (Abstr.)

Khodorov, B. I., 1978. Chemicals as tools to study nerve fiber sodium channels and effects of batrachotoxin and some local anesthetics. *In* Membrane Transport Processes. D. C. Tosteson, Yu. A. Ovchinnikov, and R. Lattore, editors. Raven Press, New York. Vol. 2.

Khodorov, B. I., B. Neumcke, W. Schwarz, and R. Stampfli. 1981. Fluctuation analysis of Na+ channels modified by batrachotoxin in myelinated nerve. *Biochim. Biophys. Acta.* 648:93–99.

Narahashi, T., E. X. Albuquerque, and T. Deguchi. 1971. Effects of batrachotoxin on membrane potential and conductance of squid giant axons. *J. Gen. Physiol.* 58:54–70.

Oxford, G. S. 1981. Some kinetic and steady-state properties of sodium channels after removal of inactivation. *J. Gen. Physiol.* 77:1–22.

Patlak, J., and R. Horn. 1982. Effect of *N*-bromoacetamide on single sodium channel currents in excised membrane patches. *J. Gen. Physiol.* 79:331–351.

Quandt, F. N., and T. Narahashi. 1982. Modification of single Na^+ channels by batrachotoxin. *Proc. Natl. Acad. Sci. USA.* 79:6732–6736.

Sigworth, F. J., and E. Neher. 1980. Single Na^+ channel currents observed in cultured rat muscle cells. *Nature (Lond.)*. 287:447–449.

Yamamoto, D., J. Z. Yeh, and T. Narahashi. 1983. Current-voltage relationship of single sodium channels in neuroblastoma cells. *Biophys. J.* 41(2,Pt.2):51 *a*. (Abstr.)

DISCUSSION

Session Chairman: Charles F. Stevens *Scribe*: Jacquiline Tanaka

HORN: You state that the open time of a BTX-modified channel is longer than that of the control. Would you describe the magnitude and voltage dependence of the unmodified channel?

HUANG: The open time of the BTX-modified channel is 5 to 10 times longer than the open time of the normal channel. We haven't characterized the complete voltage dependence of the normal channel.

NARAHASHI: Do you assume that your model holds for normal channels as well as BTX-modified channels?

HUANG: This model is just for modified channels. The normal sodium channel is very complicated.

NARAHASHI: I think the BTX channel is even more complicated.

HUANG: There are several closed states for the normal sodium channel. In our BTX model, there is no inactivation and only two closed states.

NARAHASHI: What is your single channel conductance? You mentioned 11 pS in modified channels. Did you measure normal channels?

HUANG: Our preliminary data indicate that the normal channel is 12–14 pS, so the conductance of BTX-modified channels is ~70% of the conductance of normal channels.

NARAHASHI: Our data (Yamamoto, Yeh, and Narahashi) agree with yours that BTX decreases single channel conductance but we find a more drastic effect which may be related to the cell line or the concentration of Ca^{++}. The concentration of Ca^{++} we used was higher than that in your studies but I think this only partially accounts for the discrepancy.

HUANG: Right. If there is some Ca^{++}-blocking in the channel, the single channel conductance you see may be smaller. I noticed in your studies you used 5% ethanol, which is quite high. In preliminary measurements I made with high concentrations of ethanol, the channel seems to have a large fraction of closed times. Also there seems to be a second population of channels with smaller conductance.

MILLER: Is there any process in the sodium channel that is unmodified by BTX?

HUANG: Yes, TTX blockage. Both gating properties and selectivity properties show changes.

HARTSHORNE: Do you see any difference in the voltage dependence of activation between a cell-attached and an excised patch preparation?

HUANG: All of these are cell-attached preparations.

RUDY: In response to Chris Miller's question, isn't it true that the voltage dependence is shifted but the gating charge is the same?

HUANG: Yes, you are correct. Thank you.

FINKELSTEIN: What was the voltage dependence of the closing rate time constant, i.e., the transition from open to the first closed state? What was its slope?

HUANG: It was ~17 mV for an *e*-fold change in rate, corresponding to ~1 1/2 charges crossing the membrane.

FRENCH: You see that the channel is open only ~80% of the time even at very positive potentials. In our bilayers at the bandwidth we use, we saw the channels open 98% of the time. Is there any evidence that this discrepancy may arise from using different preparations?

HUANG: I think Furman, Tanaka, and Barchi have measured an 80% open time in reconstituted sodium channels at depolarized potentials.

BARCHI: That's true but the measurements were made on a limited number of observations on a purified channel in a very different lipid environment. I'm not sure the measurements are comparable.

NARAHASHI: You mentioned that you used a patch containing only one channel as evidenced by the absence of two simultaneous openings. Can you distinguish between one channel opening repetitively and two channels opening consecutively?

HUANG: The channel should be open 80% of the time at depolarized potentials. It is hard to envision more than one channel in depolarized regions without an overlap of channels.

YEH: Have you ever used a patch having two channels, allowing you to observe one modified and one unmodified channel, as Quandt and Narahashi have?

HUANG: From our experimental protocol, the chance of seeing unmodified channels is unlikely for two reasons. First, we saturate the cell with BTX and secondly we measure steady-state currents and not pulses. Often we have 2–3 BTX channels in a patch, but I would expect any unmodified channels to be inactivated.

STEVENS: Did I understand that you actually have more than one channel in a patch but only one is modified and the others are inactivated?

HUANG: When we do steady-state measurements I don't know whether we have any normal channels because we can see only modified channels. We see two channels in 50% to 60% of the patches.

STEVENS: I expect that you are losing some channels because we see ~1% patches with a single channel. Once we had a patch with two channels and one dropped out. Perhaps in your case you can modify one channel and the others are lost.